NUCL SCI TECH (2021) 32:101
https://doi.org/10.1007/s41365-021-00931-w

Measurements of the ^{197}Au(n, γ) cross section up to 100 keV at the CSNS Back-n facility

Xin-Rong Hu[1,2] · Gong-Tao Fan[3] · Wei Jiang[4,5] · Jie Ren[6] · Long-Xiang Liu[3] · Hong-Wei Wang[2,3] · Ying-Du Liu[7] · Xin-Xiang Li[1,2] · Yue Zhang[4,5] · Zi-Rui Hao[1,2] · Pan Kuang[1,2] · Xiao-He Wang[1] · Ji-Feng Hu[1] · Bing Jiang[1,2] · De-Xin Wang[8] · Suyalatu Zhang[8] · Zhen-Dong An[9] · Yu-Ting Wang[10] · Chun-Wang Ma[10] · Jian-Jun He[11] · Jun Su[11] · Li-Yong Zhang[11]

Received: 1 February 2021 / Revised: 17 June 2021 / Accepted: 20 June 2021 / Published online: 13 September 2021
© China Science Publishing & Media Ltd. (Science Press), Shanghai Institute of Applied Physics, the Chinese Academy of Sciences, Chinese Nuclear Society 2021

Abstract The neutron capture cross section of ^{197}Au was measured using the time-of-flight (TOF) technique at the Back-n facility of the China Spallation Neutron Source (CSNS) in the 1 eV to 100 keV range. Prompt γ-rays originating from neutron-induced capture events were detected by four C_6D_6 liquid scintillator detectors. Pulse height weighting technology (PHWT) was used to analyze the data. The results are in good agreement with ENDF/B-VIII.0, CENDL-3.1, and other evaluated libraries in the resonance region, and in agreement with both n_TOF and GELINA experimental data in the 5–100 keV range. Finally, the resonance peaks in the energy range from 1 eV to 1 keV were fitted by the SAMMY R-matrix code.

Keywords Cross section · ^{197}Au(n, γ) · Back-n · C_6D_6 · Pulse height weighting technology

1 Introduction

Neutron-induced reactions play an essential role in the synthesis of the heavy elements of the universe, and approximately half of the chemical elements heavier than iron are produced by the slow neutron capture process (s process) in stars [1–4]. Most neutron capture cross sections are measured relative to the cross-sectional standards and normalized to absolute values. To date, the cross section of the ^{197}Au(n, γ) reaction with thermal neutron energy up to 2.5 MeV is the only capture criterion, while most neutron capture cross-sectional measurements refer to one or both energy regions [5]. Using the standard neutron capture cross-sectional data from the ENDF/B-VIII.0 database [6],

This work was supported by the National Natural Science Foundation of China (Nos. 11875311, 11905274, 11705156, and 11605097) and the Strategic Priority Research Program of the Chinese Academy of Sciences (No. XDB34030000)

✉ Long-Xiang Liu
liulongxiang@zjlab.org.cn

✉ Hong-Wei Wang
wanghongwei@zjlab.org.cn

1 Shanghai Institute of Applied Physics, Chinese Academy of Sciences, Shanghai 201800, China

2 University of Chinese Academy of Sciences, Beijing 100049, China

3 Shanghai Advanced Research Institute, Chinese Academy of Sciences, Shanghai 201210, China

4 Institute of High Energy Physics, Chinese Academy of Sciences, Beijing 100049, China

5 Spallation Neutron Source Science Center, Dongguan 523803, China

6 Key Laboratory of Nuclear Data, China Institute of Atomic Energy, Beijing 102413, China

7 Xiangtan University, Xiangtan 411105, China

8 Institute of Nuclear Physics, Inner Mongolia University for the Nationalities, Tongliao 028000, China

9 Sun Yat-sen University, 510275 Zhuhai, China

10 Henan Normal University, Xinxiang 453007, China

11 Beijing Normal University, 100875 Beijing, China

we can check the feasibility of our experimental setup and method.

We use the C_6D_6 detector system to measure the decay of gamma rays emitted from the compound nucleus owing to its low sensitivity to neutrons and short response time [7]. The ^{197}Au(n, γ) cross section was measured from 1 eV to 100 keV owing to the influence of the gamma flash from a white neutron source at high neutron energy regions. We then analyzed the experimental data using the pulse height weighting technique (PHWT), and compared our experimental data with the evaluation data of the evaluated nuclear data file (ENDF). Finally, we used SAMMY code [8] to fit the experimental data in the resonance energy range from 1 eV to 1 keV and extracted the corresponding resonance parameters.

The remainder of this paper is organized as follows: a detailed introduction of the C_6D_6 detector system at Back-n is given in Sect. 2. The raw data analysis using the PHWT method for neutron capture cross sections is presented in Sect. 3. Finally, conclusions and uncertainty analysis are presented in Sect. 4.

2 Measurements

The China Spallation Neutron Source (CSNS) [9, 10] is the first spallation neutron source facility that provides a pulsed neutron beam with energy from thermal energy to 400 MeV in China [11, 12]. The neutron beam is produced through the pulses of protons with an energy of 1.6 GeV and a pulse frequency of 25Hz, bombarding a tungsten (W) target. The Back-n white neutron beamline is constructed 180° to the proton beam direction, and the neutron flux can reach up to 10^7 n/cm^2/s at the experimental station (ES). There are two experimental stations on the Back-n beamline, as shown in Fig. 1; ES#1 is approximately 55 m from the spallation target, which mainly studies the (n, lcp (light charge particle)) reaction cross section, and ES#2 is approximately 76 m, which is mainly for the measurements of (n, γ), (n, *tot*), and (n, *f*) reactions cross sections [13–16].

2.1 The C_6D_6 detector system in Back-n neutron beamline

The Back-n C_6D_6 detector system consists of four C_6D_6 liquid scintillation detectors, one aluminum detector's brackets, and one aluminum sample holder, as shown in Fig. 2. The C_6D_6 detectors are placed upstream of the neutron beam sample target to decrease the elastic scattering neutron background, and the detector axis is at an angle of 110 °from the neutron beam. The distance between the C_6D_6 detectors front center to the sample target center was 150 mm and 80 mm from the neutron beam axis.

The C_6D_6 detector is a liquid scintillator EJ315 [17] produced by the ELJEN Technology Corporation. The shell of the scintillator shell is made of aluminum owing to its low capture rate, with a diameter and length of 130 mm and 76.2 mm, respectively. The structure of the detector system used in the Geant4 simulation is shown in Fig. 3.

In the neutron capture cross-sectional measurements, the amplitude of the anode signals of the C_6D_6 detectors is from 0.01 to 3 V. Signals from the C_6D_6 detectors are delivered to the readout electronics, which can digitize the analog signals into a full waveform with a 1 GS/s sampling rate and 12 bits resolution [18]. The neutron start time T_0 signals are picked up by the pulsed proton beam, while the stop time T_S of the neutrons that have reacted in the sample is picked up by the C_6D_6 detectors; further, the electronics record these signals so that the incident neutron energy can be determined using the time-of-flight (TOF) technique. The energy of the incident neutron (E_n) is given by Eq. (1), and the neutron energy resolution is calculated using Eq. (2) [19],

$$E_n = \frac{1}{2} m_n v^2 = \left(\frac{72.2977L}{tof}\right)^2, \tag{1}$$

$$\frac{\Delta E_n}{E_n} = 2\sqrt{\left(\frac{\Delta L}{L}\right)^2 + \left(\frac{\Delta tof}{tof}\right)^2}, \tag{2}$$

where the flight length $L = L_0 + \Delta L(E_n)$, L_0 is the geometric distance from the spallation target to the sample, and $\Delta L(E_n)$ is the equivalent change in moderation length associated with the incident neutron energy. E_n, L, and $tof = T_S - T_0$ are in units of MeV, m, and ns, respectively.

In addition, the setup of the capture measurements is complemented by a silicon flux monitor (SiMon); the SiMon consists of a thin ^{6}LiF conversion layer and eight silicon detectors outside the neutron beam (Li-Si Monitor) to count the number of neutrons by detecting alpha particles and ^{3}H through the reaction ^{6}Li(n, α)^{3}H [20].

2.2 Samples

The gold sample(Au) with $\Phi 50\,\mathrm{mm} \times 1\,\mathrm{mm}$, natural C sample with $\Phi 50\,\mathrm{mm} \times 1\,\mathrm{mm}$, and natural Pb sample (an additional experiment with a proton power of 80 kW) with $\Phi 30\,\mathrm{mm} \times 0.53\,\mathrm{mm}$ are shown in Table 1. The ^{nat}C and empty samples were used for background subtraction in our experiment because of sample scattered neutrons and γ rays from the surroundings, and the ^{nat}Pb sample was used for subtracting the in-beam γ-ray background.

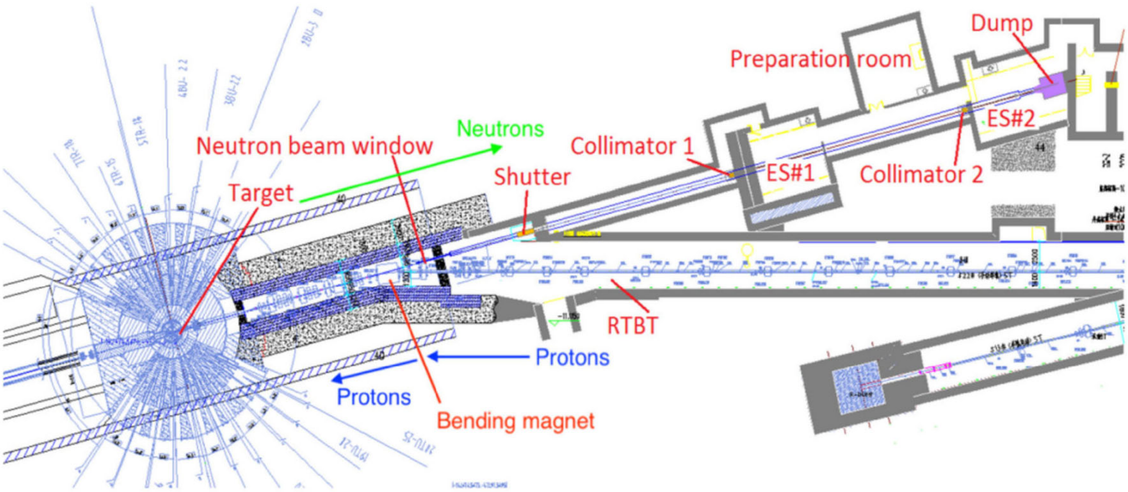

Fig. 1 (Color online) Layout of the Back-n beam line at CSNS

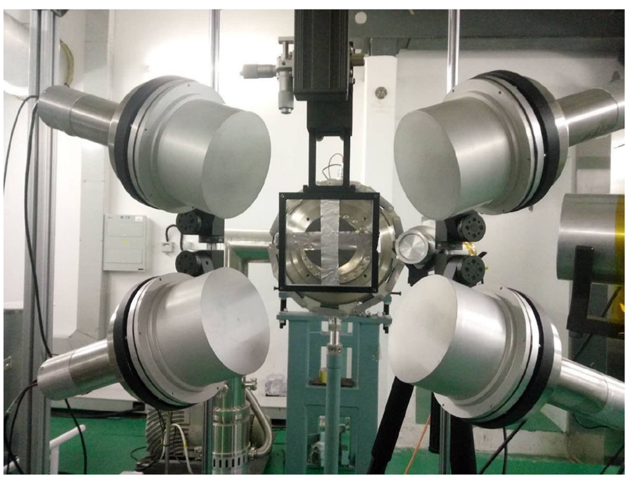

Fig. 2 (Color online) Photograph of the C_6D_6 detector system

3 Analysis of the C_6D_6 data

The C_6D_6 detector system is one of the total energy detection systems primarily used for neutron capture cross-sectional measurements [19]. Because of the low detection efficiency of γ rays and the detection efficiency being directly proportional to the γ ray energy, the pulse height weighting technique (PHWT) was used in the data analysis.

3.1 From measured count rate to capture yield

The experimental yield Y_{exp} is obtained as a function of the neutron energy E_{n} from the weighed rate N_{W} through the PHWT [21, 22]

$$Y_{\mathrm{exp}} = f_{\mathrm{N}} \frac{N_{\mathrm{W}}}{IE_{\mathrm{c}}}, \tag{3}$$

where Y_{exp}, N_{W}, and the neutron intensity I depend on the TOF or neutron energy; the weighted count rate N_{W} is

Fig. 3 (Color online) C_6D_6 detector system structure by Geant4 simulation

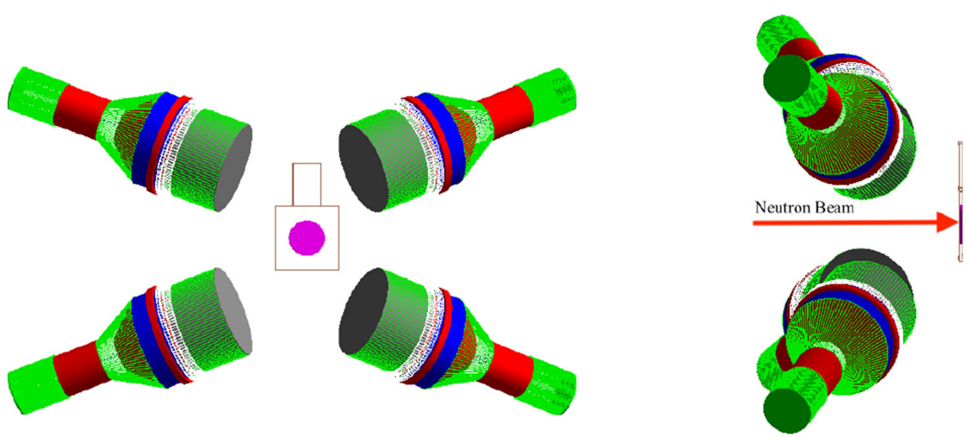

Table 1 The gold(Au), carbon(C) and lead(Pb) samples used for the capture measurement

Sample	Diameter (mm)	Thickness (mm)	Weight (g)	Area (cm^2)	Area density Atoms/Barn
^{197}Au	50	1	37.93	19.63	5.907×10^{-3}
^{nat}C	50	1	4.42	19.63	1.128×10^{-2}
^{nat}Pb	30	0.53	4.24	7.07	1.748×10^{-3}
Empty target	–	–	–	–	–

described in the following sections. The neutron intensity $I(E_\mathrm{n})$ is proportional to the total number of neutrons interacting with the sample with energy E_n, as shown in Fig. 4. The fixed fraction f_N is the yield normalization factor for flux calibration, which was normalized to one at 4.9 eV owing to the saturated resonance of the thick gold sample. E_C represents the total capture energy, which for the kinetic energy E_n of the center-of-mass frame is given by $E_\mathrm{C} = E_\mathrm{n} + S_\mathrm{n}$, where $S_\mathrm{n} = 6.512$ MeV is the neutron separation energy of the compound nuclei ^{198}Au.

3.2 Pulse height weighting technique

In 1963, Moxon and Rae [24] first proposed the principle of the PHWT and constructed a simple gamma detector consisting of a carbon disk and a thin plastic scintillator. Macklin and Gibbons [25] first applied a pair of C_6F_6 detectors to neutron capture cross-sectional studies in 1967. Using this technique, the detection efficiency is proportional to the gamma energy; thus, $\epsilon_\gamma = c \cdot E_\gamma$. Because $\epsilon_\gamma \ll 1$ and $E_\mathrm{C} = E_\mathrm{n} + S_\mathrm{n}$, the capture efficiency ϵ_C can be written as [7]

$$\epsilon_\mathrm{C} = 1 - \prod_{i=1}^{N}(1-\epsilon_{\gamma_i}) \simeq \sum_{i=1}^{N}\epsilon_{\gamma_i} = c\sum_{i=1}^{N}E_{\gamma_i} = c\cdot(E_\mathrm{n}+S_\mathrm{n}).$$

To validate the equation, we introduced the weighting function (WF)$W(E_i)$ as follows:

$$W(E_i) = \sum_{k=0}^{4} a_k E_i^{\,k}. \tag{4}$$

The WFs used for the present measurements were obtained from the response functions of mono-energetic γ-rays, which were calculated using Monte Carlo simulations of the experimental setup with Geant4.10.06 [26–28]. The simulated γ-rays with energies ranging from 0.15 to 7 MeV were produced from the volume (surface) of the gold sample, and then emitted homogeneously; further, part of the gamma ray was deposited energy in the C_6D_6 detectors. The simulated γ-ray energy deposition spectrum or pulse height (PH) spectrum is shown in Fig. 5; the energy threshold was 100 keV. Moreover, the original detection efficiency of the primary C_6D_6 setup is approximately 2%, the weighted efficiency has a fixed linear relationship with

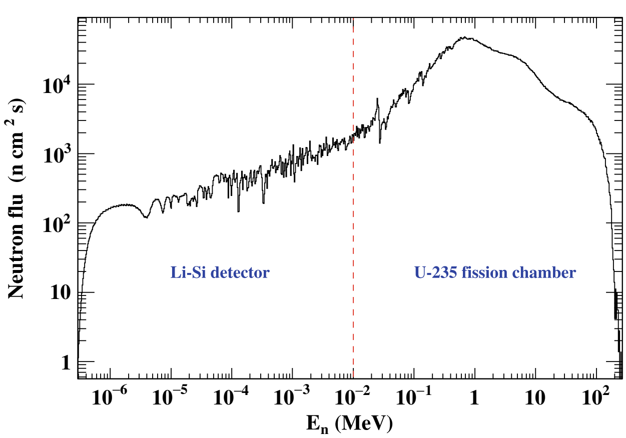

Fig. 4 (Color online)Neutron spectrum of the experimental station (ES) at the Back-n neutron beamline. The neutron spectrum below 10 keV was measured using a Li-Si detector, while above 10 keV was measured using the U-235 fission chamber, and more detailed measurements have been discussed by Chen *et al.* [23]

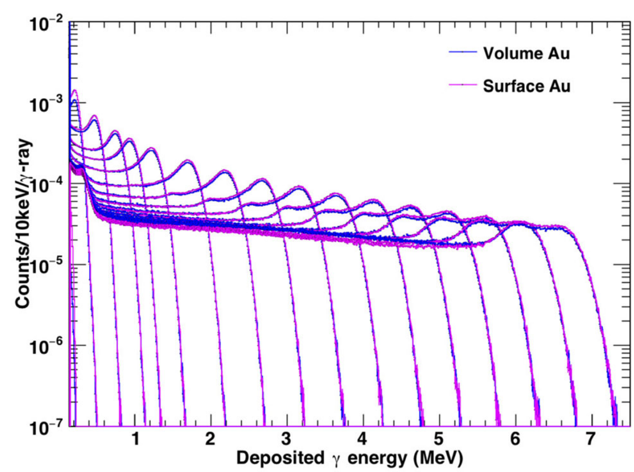

Fig. 5 (Color online)PH spectrum of ^{197}Au simulated using Geant4 with energy broadening. The blue line represents the γ-rays emitted from the volume of the sample, and the purple line represents the γ-rays emitted from the front surface of the sample

γ-ray energy, and the ratios of each energy point are very close to those shown in Fig. 6a. We compared the γ-rays emitted from the volume of the gold sample and from the surface of the sample, and there was little difference between the two modes of emissions.

The χ^2 method is applied to ensure that the WF parameters a_k use gamma-ray energy ranging from 0.15 to 7 MeV, as shown in Eq. (5) or Eq. (6)

$$\chi^2 = \sum_i \left[cE_{\gamma j} - \int_{E_L}^{\infty} R(E_{\rm d}, E_{\gamma j}) W(E_{\rm d}) {\rm d}E_{\rm d} \right]^2, \tag{5}$$

$$\chi^2 = \sum_{j=1}^{16} \left[\sum_{i=0}^{700} \sum_{k=0}^{4} a_k ((i-0.5)\Delta E)^k R_i^j - E_{\gamma j} \right]^2. \tag{6}$$

Usually, the constant factor c is set to one, and $R(E_{\rm d}, E_{\gamma j})$ or R_i^j is the response function of the detectors of the $j_{\rm th}$ γ-rays with an energy of $E_{\gamma j}$ from the Geant4 simulation, $E_{\rm d}$ is the deposition gamma energy, and ΔE denotes the γ energy bin width of 10 keV. The weight function is solved by the ROOT Minuit method shown in Fig. 6b.

3.3 From capture yield to cross section

In the experiment, we measured data from the gold sample, carbon sample to subtract the elastic scattering contribution, empty sample (beamOn) to subtract the ambient background, and lead sample to subtract the in-beam γ background. The raw counts from the experiment shown in Fig. 7a were normalized to the SiMon rate. The experimental capture yield, as shown in Fig. 7b, was normalized to a single neutron using the counts of the SiMon detectors. The weighted counts $N_{\rm W}$ of the gold sample were deduced from the ambient background through the empty sample (beam on), neutron elastic scattering background through the carbon sample, and in-beam γ-ray background through the natural lead sample, as expressed by Eq. (7), where $N_{\rm net}$, $N_{\rm Bkg}$, $N_{\rm C}$, and $N_{\rm Pb}$ are the sample counts after subtracting the background, empty sample counts, natural carbon sample counts, and natural Pb sample counts, respectively. W is the weighting function of the detector system, and η is directly proportional to the product of the number of target nuclei per unit area and the elastic scattering cross section of the sample. In theory, the multiple scattering and self-shield-corrected capture yield [5, 21] is related to the capture cross section $\sigma_{\rm C}$, total cross section $\sigma_{\rm t}$ (from ENDF's evaluated database), density of the sample n, thickness of the sample t, and fixed factor $f_{\rm C}$ of the sample thickness, which is related to the capture cross sections, as shown in Eq. (8).

$$N_{\rm W} = N_{\rm net} \cdot W = [N_{\rm sample} - N_{\rm Bkg} - \eta(N_{\rm C} - N_{\rm Bkg}) - N_{\rm Pb}] \cdot W \tag{7}$$

$$Y_{\rm th}(E_{\rm n}) = (1 - e^{-n t \sigma_t(E_{\rm n}) f_{\rm C}}) \frac{\sigma_{\rm C}(E_{\rm n})}{\sigma_{\rm t}(E_{\rm n})} \tag{8}$$

Then, combined with the experimental capture yield $Y_{\rm exp}(E_{\rm n})$, the present experimental capture cross-sectional formula is as follows:

$$\sigma_{\rm C}(E_{\rm n}) = \frac{\sigma_{\rm t}(E_{\rm n})}{1 - e^{-nt\sigma t(En) f c}} Y_{\rm exp}(E_{\rm n}). \tag{9}$$

Considering the multi-elastic scattering of neutrons in the thick sample, we introduced the factor $f_{\rm C}$, which is related to the sample's absorption cross section and the thickness of the sample. The factor $f_{\rm C}$ is defined in Eq. (10). It is the ratio of the mean neutron transmission length $\overline{L}$ (the addition of all step lengths extracted from the Geant4 simulation) to the target thickness t.

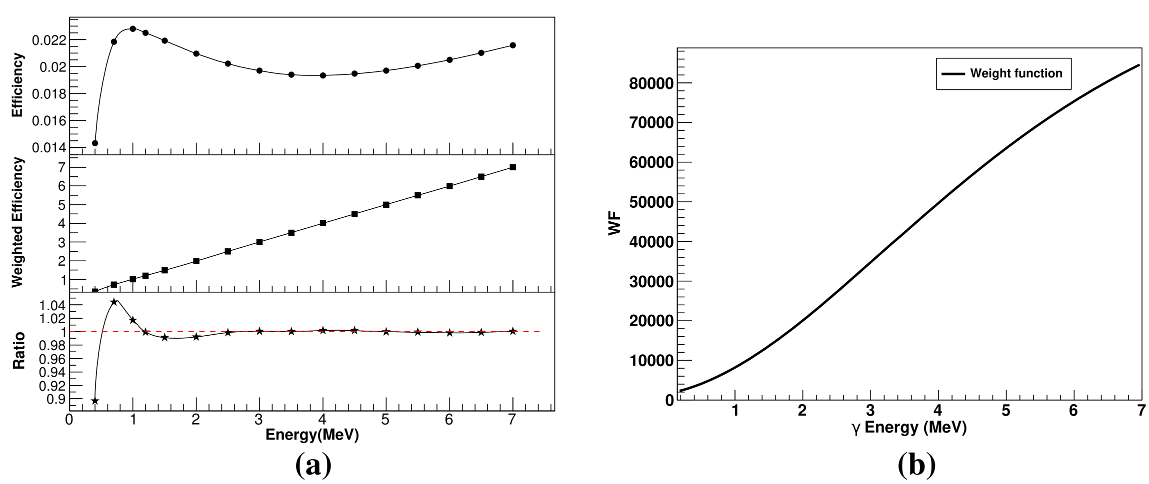

Fig. 6 (Color online) **a** The original efficiency of the C_6D_6 detectors setup in the top tile, the weighted efficiency of the setup shown in the middle tile, and the ratio between weighted efficiency and the corresponding γ energy in the bottom tile, which is very close to one. **b** The weighting function of the ^{197}Au sample

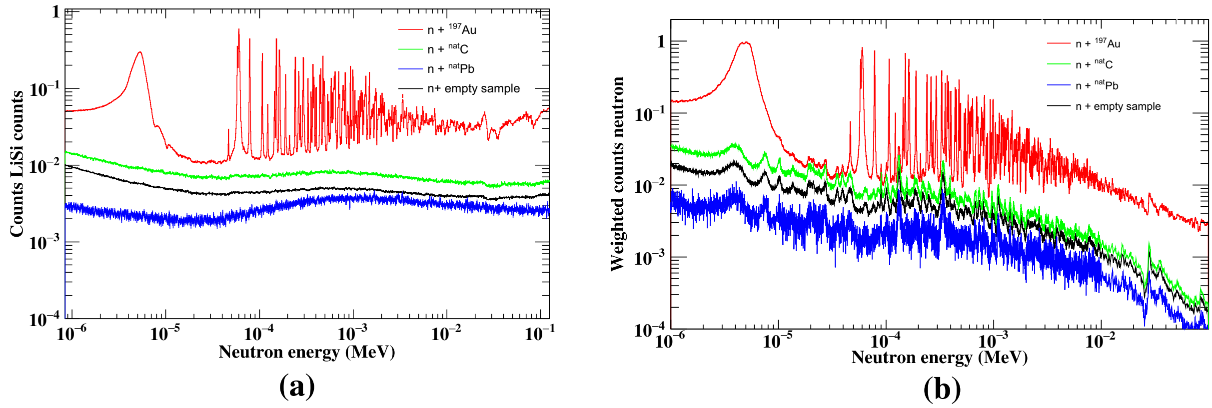

Fig. 7 (Color online) **a** The count rates of the experimental samples were normalized using a Li-Si Monitor, and the count rates are expressed in a width-independent logarithmic equidistant binning. **b** The experimental yield of different samples was normalized using a Li-Si monitor

$$f_C = \bar{L}/t \tag{10}$$

Figure 8 shows the Geant4 simulated results of gold targets with thicknesses of 0.1 mm and 1 mm and neutrons with energy in the range from 0.1 eV to 100 keV. The negative peaks show strong resonance absorption, such as 4.9 eV (the first resonance peak in ^{197}Au target). The regions of the positive peaks indicate that neutrons multi-scattered in those elastic scattering energy regions. Thus, the sufficient thickness of the sample ($\bar{L}$) is larger than the thickness of the target when the factor f_C larger than one.

4 Conclusions and uncertainty analysis

The ^{197}Au(n, γ) reaction cross section was experimentally measured with neutrons with energy from 1 eV to 100 keV, and the results were in good agreement with the latest ^{197}Au standard evaluated capture cross sections ENDF/B-VIII.0 [29], CENDL-3.1 [30], and JENDL-4.0 [31] in the entire tested energy region, as shown in Fig. 9. More detailed results in the resolved resonance region(RRR) are shown in Fig. 10a and b, which indicates that this work has a good energy resolution. Among the peak values of the energy points, the present results are larger than those of the ENDFs owing to the background in the experiment, which cannot be deducted completely [32–35]. Figure 10c indicates that there are many resonances in the region of 2–5 keV in the experimental data, as well as in the CENDL-3.1 data, while the average cross-sectional data are still used in the ENDF/B-VIII.0 database for this region. In addition, the present data in the unresolved resonance region (URR) from 10 keV to 100 keV are generally in agreement with those of the evaluated databases, Lederer's data [36] in 2011 and Massimi's data [37] in 2014 shown in Fig. 10d. Finally, the R-matrix code SAMMY(R6) [8] in the Reich–Moore multi-level approximation was used to analyze the resonance shape of the capture cross section in the energy region from 1 eV to 1 keV. The analysis included self-shielding and multiple corrections, and Doppler broadening with an effective temperature of 300 K using the free gas model (FGM). The R-matrix fitting

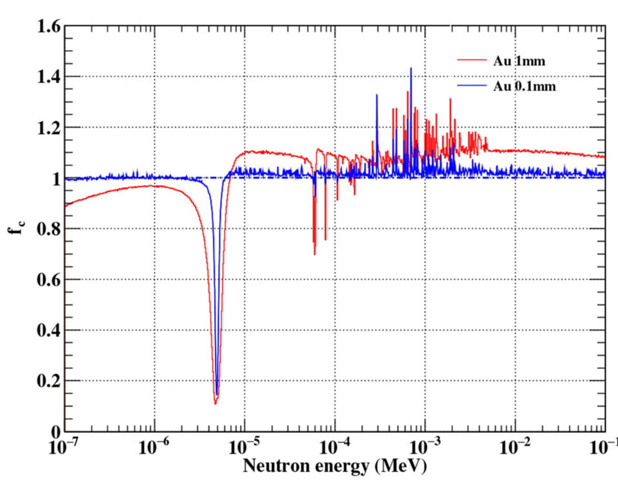

Fig. 8 (Color online) The multiple scattering correction factor of f_C for 0.1 mm and 1 mm thickness gold samples

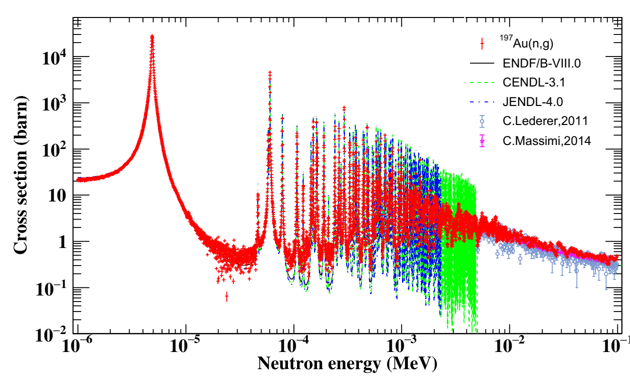

Fig. 9 (Color online) Neutron capture cross section of ^{197}Au in the region from 1 eV to 100 keV

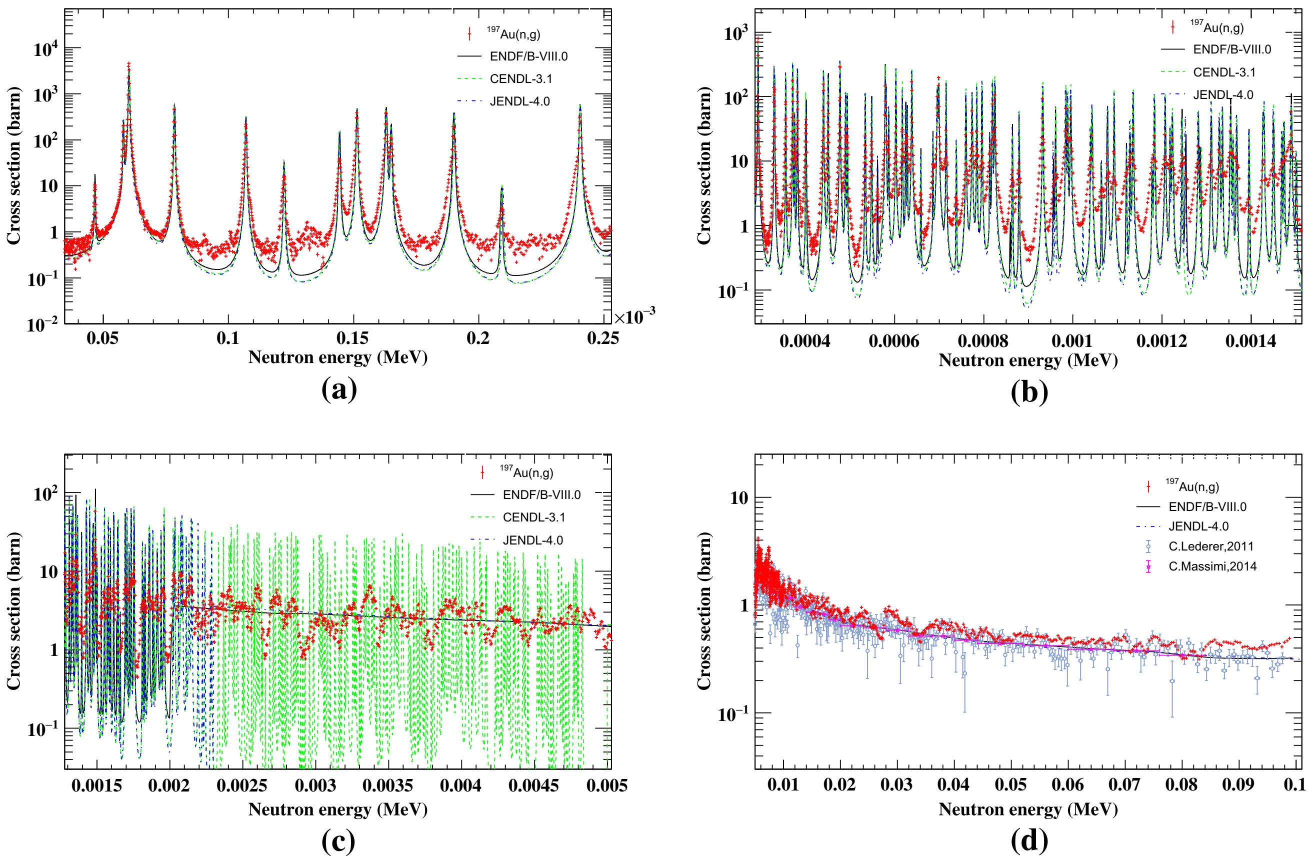

Fig. 10 (Color online) **a**, **b** Neutron capture cross section of ^{197}Au in resonance regions. **c** Neutron capture cross section of ^{197}Au in the region of 1–5 keV. **d** Neutron capture cross section of ^{197}Au in the unresolved resonance region of 10–100 keV

results were in agreement with the experimental data shown in Fig. 11). The fitting resonance parameters of the resonance energy (E_R), gamma width (Γ_γ), and neutron width (Γ_n) are listed in Table 2.

The ^{197}Au(n, γ) neutron capture cross section was measured at the Back-n neutron beamline of the CSNS, which is aimed at verifying the rationality of the new C_6D_6 setup for neutron capture cross-sectional measurements. The results are found to be in good agreement with those of the ENDFs and other evaluation data and the n_TOF experimental data, especially in the resonant energy region. The statistical uncertainty of the measured ^{197}Au(n, γ) reaction cross section is less than 2%, while the other uncertainties come from the background that is removed through the carbon and empty targets, and from the energy dependence of the neutron flux, which is the largest contribution with approximately 5% at present [23]. The other uncertainties are due to the PHWT and were 2–3%, as shown in Ref. [38]. The results show that the C_6D_6 detectors and PHWT detection technology in the Back-n neutron beamline of CSNS is an effective detection system for capture cross-sectional measurements that are >100 mb, especially for the 1 eV to 100 keV low resonance energy regions.

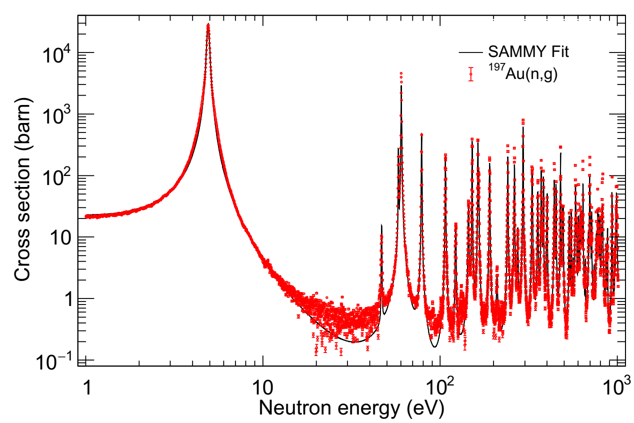

Fig. 11 (Color online) Resolved resonance range of 1 eV–1 keV analyzed in this work. The red points are the experimental data, and the black line represents the R-matrix fit

Table 2 Resonance parameters extracted from the R-matrix analysis of the experimental data

E_R (eV)	l	J^π	Γ_γ (meV)			Γ_n (meV)		
			This work	ENDF/B-VIII.0	n_TOF	This work	ENDF/B-VIII.0	n_TOF
4.904	0	2^+	119.0	121.4	124.0	16.01	14.96	15.2
46.70	0	1^+	132.0	127.0	128.0	0.190	0.220	0.223
58.08	0	1^+	111.7	113.0	112.0	4.55	4.31	4.34
60.31	0	2^+	113.5	118.0	110.0	88.80	70.66	73.9
78.53	0	1^+	118.5	124.0	120.0	25.59	17.00	17.79
107.04	0	2^+	110.2	123.0	110.0	10.31	7.83	8.29
122.25	0	2^+	128.0	121.0	128.0	0.730	0.900	0.86
144.46	0	1^+	121.0	121.0	120.0	3.90	9.07	9.35
151.42	0	2^+	150.0	121.0	150.0	36.15	22.26	21.6
163.13	0	1^+	197.0	129.0	197.0	67.88	55.16	42.5
165.25	0	2^+	109.0	121.0	109.0	7.17	9.98	8.67
190.04	0	1^+	132.0	121.0	130.0	58.98	49.08	49.8
209.21	0	1^+	178.0	121.0	180.0	0.473	0.860	0.860
240.65	0	2^+	99.6	121.0	99.6	74.17	74.16	86.6
255.82	0	1^+	124.0	124.0	130.0	0.204	0.561	0.500
262.26	0	1^+	129.0	129.0	124.0	325.6	144.0	152.0
273.95	0	2^+	121.0	121.0	110.0	1.58	4.83	4.41
293.56	0	2^+	135.7	126.0	123.6	587.2	364.0	348.0
329.39	0	2^+	137.0	137.0	137.0	31.56	46.0	41.5
330.92	0	1^+	130.0	130.0	130.0	45.19	62.18	56.2
355.25	0	2^+	125.0	125.0	125.0	24.46	40.00	37.6
371.36	0	2^+	121.0	121.0	99.0	289.7	85.88	109.0
376.20	0	1^+	121.0	121.0	125.0	4.77	13.92	12.3
382.13	0	2^+	98.0	121.0	97.0	45.15	63.11	73.9
400.27	0	2^+	128.0	128.0	128.0	6.83	6.83	6.08
401.68	0	1^+	140.0	140.0	140.0	19.35	26.96	25.8
440.45	0	1^+	150.0	150.0	149.0	650.5	297.3	281.4
451.15	0	2^+	111.0	128.6	110.0	28.14	63.50	63.7
477.60	0	2^+	124.0	137.1	124.9	927.0	317.0	296.1
489.90	0	1^+	138.0	138.0	138.0	17.68	60.83	62.2
493.98	0	2^+	110.0	121.0	111.0	10.36	28.16	28.5
534.13	0	2^+	130.0	130.0	130.0	9.01	66.01	31.8
548.58	0	1^+	128.0	121.0	127.0	19.45	62.14	58.6
561.68	0	2^+	128.0	128.0	128.0	3.36	2.95	2.44
579.26	0	2^+	126.6	155.6	126.0	647.2	358.7	288.4
581.16	0	1^+	123.0	114.7	122.0	306.8	146.2	306.8
586.84	0	2^+	134.0	134.0	134.0	22.86	23.86	22.4
602.99	0	2^+	112.5	119.5	113.0	42.70	227.4	223.9
617.37	0	1^+	313.6	127.5	135.0	128.3	128.3	111.0
624.72	0	1^+	121.0	121.0	121.0	20.8	30.86	53.4
628.23	0	2^+	138.0	121.0	138.0	11.55	50.15	24.7
638.96	0	2^+	120.0	132.1	118.5	510.7	510.6	464.0
659.16	0	2^+	97.0	97.0	97.0	1.04	4.84	4.20
686.27	0	1^+	128.0	128.0	128.0	6.64	19.89	16.8
696.04	0	1^+	142.5	159.1	139.0	699.8	716.4	666.7
699.44	0	2^+	244.2	111.3	110.0	800.0	699.8	736.1

Table 2 continued

E_R (eV)	l	J^π	Γ_γ (meV)			Γ_n (meV)		
			This work	ENDF/B-VIII.0	n_TOF	This work	ENDF/B-VIII.0	n_TOF
715.88	0	2^+	112.0	121.0	112.0	17.96	114.4	110.0
738.72	0	1^+	120.0	120.0	120.0	1.76	12.08	10.6
760.16	0	1^+	113.0	119.0	110.0	34.97	411.6	426.7
774.04	0	1^+	127.0	136.0	125.0	480.9	431.9	474.6
784.62	0	2^+	140.0	140.0	140.0	20.74	110.3	14.0
796.40	0	2^+	124.0	142.0	123.0	178.0	157.8	177.6
813.81	0	1^+	128.0	128.0	128.0	15.46	24.11	22.1
819.78	0	2^+	128.0	128.0	128.0	240.0	253.9	232.0
825.56	0	2^+	155.3	134.8	117.0	560.0	523.1	426.4
864.10	0	2^+	121.0	121.0	107.0	4.90	20.94	18.4
879.18	0	2^+	66.0	121.0	66.0	6.43	30.92	35.2
932.61	0	2^+	126.0	134.7	124.0	754.2	429.8	340.0
956.27	0	2^+	128.0	121.0	128.0	2.40	6.18	6.30
961.51	0	2^+	150.0	157.3	150.0	9.01	49.2	49.2
984.85	0	2^+	125.5	116.3	94.0	586.0	327.8	250.0
988.89	0	2^+	160.0	121.0	160.0	34.28	125.2	94.0
995.81	0	2^+	131.0	121.0	130.0	505.1	505.0	350.0

Quantum numbers l and J^π are taken from ENDF/B-VIII.0

Acknowledgements The authors would like to thank colleagues from the Back-n facility as well as Prof. Gui-Lin Zhang for his advice on data analysis.

Author contributions All authors contributed to the study conception and design. Material preparation, data collection, and analysis were preformed by Hong-Wei Wang, Xin-Rong Hu, Long-Xiang Liu, and Gong-Tao Fan. The first draft of the manuscript was written by Xin-Rong Hu, and all authors commented on previous of the manuscript. All authors read and approved the final manuscript.

References

1. N. Colonna, F. Gunsing, F. Käppeler, Neutron physics with accelerators. Prog. Part. Nucl. Phys. **101**, 177 (2018). https://doi.org/10.1016/j.ppnp.2018.02.002
2. F. Käppeler, Reaction cross sections for the *s*, *r*, and *p* process. Prog. Part. Nucl. Phys. **66**, 390 (2011). https://doi.org/10.1016/j.ppnp.2011.01.040
3. F. Käppeler, R. Gallino, S. Bisterzo et al., The *s* process: nuclear physics, stellar models, and observations. Rev. Mod. Phys. **83**, 157 (2011). https://doi.org/10.1103/RevModPhys.83.157
4. C. Lederer-Woods, U. Battino, P. Ferreira et al., Measurement of ^{73}Ge(n, γ) cross sections and implications for stellar nucleosynthesis. Phys. Lett. B **790**, 458–465 (2019). https://doi.org/10.1016/j.physletb.2019.01.045
5. C. Massimi, C. Domingo-Pardo, G. Vannini et al., ^{197}Au(n, γ) cross section in the resonance region. Phys. Rev. C **81**, 044616 (2010). https://doi.org/10.1103/PhysRevC.81.044616
6. Evaluated nuclear data file (ENDF). https://www.nndc.bnl.gov/exfor/endf00.jsp
7. A. Borella, G. Aerts, F. Gunsing et al., The use of C_6D_6 detectors for neutron induced capture cross-section measurements in the resonance region. Nucl. Instr. Methods A **577**, 626 (2007). https://doi.org/10.1016/j.nima.2007.03.034
8. N. M. Larson, Updated Users' Guide for SAMMY: Multilevel R-matrix Fits to Neutron Data Using Bayes' Equations. Oak Ridge National Laboratory Report No. /TM-9179/R6
9. H.S. Chen, X.L. Wang, China's first pulsed neutron source. Nat. Mater. **15**, 689 (2016). https://doi.org/10.1038/nmat4655
10. L.P. Zhou, Q.L. Mu, H.T. Jing et al., A possible scheme for the surface muon beamline at CSNS. Nucl. Sci. Tech. **30**, 169 (2019). https://doi.org/10.1007/s41365-019-0648-1
11. J.Y. Tang, S.N. Fu, H.T. Jing et al., Proposal for muon and white neutron sources at CSNS. Chin. Phys. C **34**, 121 (2010). https://doi.org/10.1088/1674-1137/34/1/022
12. X.M. Jin, Y. Liu, C.L. Su et al., Ionizing and non-ionizing kerma factors in sillicon for China Spallation Neutron Source neutron spectrum. Nucl. Sci. Tech. **30**, 143 (2019). https://doi.org/10.1007/s41365-019-0664-5
13. Q. An, H.Y. Bai, J. Bao et al., Back-n white neutron facility for nuclear data measurements at CSNS. J. Instrum. **12**, P07022 (2017). https://doi.org/10.1088/1748-0221/12/07/P07022
14. H.T. Jing, J.Y. Tang, H.Q. Tang et al., Studies of back-streaming white neutrons at CSNS. Nucl. Instrum. Methods A **621**, 91 (2010). https://doi.org/10.1016/j.nima.2010.06.097
15. J.Y. Tang, J.B. Bai et al., Back-n white neutron source at CSNS and its applications. Nucl. Sci. Tech. **32**, 11 (2021). https://doi.org/10.1007/s41365-021-00846-6
16. J.Y. Tang and the CSNS Back-n Collaboration, Back-n white neutron facility at CSNS and first-year nuclear data measurements. In *Proceeding of ND2019, EPJ Web of Conferences*, 239, 06002 (2020). https://doi.org/10.1051/epjconf/202023906002
17. EJ-315 deuterated liquid scintillator data sheet. https://eljentechnology.com/

18. J. Ren, X. Ruan, J. Bao et al., The C_6D_6 detector system on the Back-n beam line of CSNS. Radiat. Detect. Technol. Methods **3**, 52 (2019). https://doi.org/10.1007/s41605-019-0129-8
19. R. Reifarth, P. Erbacher, S. Fiebiger et al., Neutron-induced cross sections: from raw data to astrophysical rates. Eur. Phys. J. Plus **133**, 424 (2018). https://doi.org/10.1140/epjp/i2018-12295-3
20. T. Wright, C. Guerrero, J. Billowes et al., Measurement of the ^{238}U(n, γ) cross section up to 80 keV with the Total Absorption Calorimeter at the CERN n_TOF facility. Phys. Rev. C **96**, 064601 (2017). https://doi.org/10.1103/PhysRevC.96.064601
21. K. Fraval, F. Gunsing, S. Altstadt et al., Measurement and analysis of the ^{241}Am(n, γ) cross section with liquid scintillator detectors using time-of-flight spectroscopy at the n_TOF facility at CERN. Phys. Rev. C **89**, 044609 (2014). https://doi.org/10.1103/PhysRevC.89.044609
22. J. Lerendegui-Marco, C. Guerrero, E. Mendoza et al., Radiative neutron capture on ^{242}Pu in the resonance region at the CERN n_TOF EAR1 facility. Phys. Rev. C **97**, 024605 (2018). https://doi.org/10.1103/PhysRevC.97.024605
23. Y. Chen, G. Luan, J. Bao et al., Neutron energy spectrum measurement of the Back-n white neutron source at CSNS. Eur. Phys. J. A **55**, 115 (2019). https://doi.org/10.1140/epja/i2019-12808-1
24. M.C. Moxon, E.R. Rae, A gamma-ray detector for neutron capture cross-section measurements. Nucl. Instrum. Methods **24**, 445 (1963). https://doi.org/10.1016/0029-554X(63)90364-1
25. R.L. Macklin, J.H. Gibbons, Capture-cross-section studies for 30–220 keV neutrons using a new technique. Phys. Rev. **159**, 1007 (1967). https://doi.org/10.1103/PhysRev.159.1007
26. S. Agostinelli, J. Allison, K. Amako et al., Geant4: a simulation toolkit. Nucl. Instrum. Methods A **506**, 250 (2003). https://doi.org/10.1016/S0168-9002(03)01368-8
27. J. Allison, K. Amako, J. Apostolakis et al., Geant4 developments and applications. IEEE Trans. Nucl. Sci. **53**, 270–278 (2006). https://doi.org/10.1109/TNS.2006.869826
28. J. Allison, K. Amako, J. Apostolakis et al., Recent developments in Geant4. Nucl. Instrum. Methods A **835**, 186–225 (2016). https://doi.org/10.1016/j.nima.2016.06.125
29. I. Sirakov, S. Kopecky, P.G. Yong, IAEA, ENDF/B-VIII.0 Database, LANL http://www-nds.iaea.org/exfor/endf.htm
30. H.R. Yuan, S.N. Wang, IAEA, CENDL-3.1 database, CNDC. http://www-nds.iaea.org/exfor/endf.htm
31. N. Iwamoto, IAEA, JENDL-4.0 database, JAEA. http://www-nds.iaea.org/exfor/endf.htm
32. J. Ren, X.C. Ruan, W. Jiang et al., Background study for (n, γ) cross section measurements with C_6D_6 detectors at CSNS Back-n. Nucl. Instrum. Methods A **985**, 164703 (2021). https://doi.org/10.1016/j.nima.2020.164703
33. J. Ren, X.C. Ruan, Y.H. Chen et al., In-beam γ-rays of back-streaming white neutron source at China Spallation Neutron Source. Acta Physica Sinica **69**(17), 172901 (2020). https://doi.org/10.7498/aps.69.20200718 **(in Chinese)**
34. X.X. Li, L.X. Liu, W. Jiang et al., Neutron capture cross section measurement of ^{197}Au with pulse height weighting techniques. Nucl. Tech. **43**(8), 080501 (2020). https://doi.org/10.11889/j.0253-3219.2020.hjs.43.080501 **(in Chinese)**
35. X.Y. Liu, Y.W. Yang, R. Liu et al., Measurement of the neutron total cross section of carbon at the Back-n white neutron beam of CSNS. Nucl. Sci. Tech. **30**, 139 (2019). https://doi.org/10.1007/s41365-019-0660-9
36. C. Lederer, N. Colonna, C. Domingo-Pardo et al., ^{197}Au(n, γ) cross section in the unresolved resonance region. Phys. Rev. C **83**, 034608 (2011). https://doi.org/10.1103/PhysRevC.83.034608
37. C. Massimi, B. Becker, E. Dupont et al., Neutron capture cross section measurements for ^{197}Au from 3.5 to 84 keV at GELINA. Eur. Phys. J. A **50**, 124 (2014). https://doi.org/10.1140/epja/i2014-14124-8
38. J.L. Tain, F. Gunsing, D. Aniel-Cano et al., Accuracy of the pulse height weighting technique for capture cross section measurements. J. Nucl. Sci. Technol. **39**, 689 (2002). https://doi.org/10.1080/00223131.2002.10875193